to electrochemical migration (corrosion) in the presence of both electrical bias and moisture [1-2]. There are two kinds of corrosions in electronic packages. The first kind is the metal dentritic growth at the cathode side on the surface of substrate (e.g. copper trace). Electrolytic dissolution of copper at anode will create metal ions. The metal ions then migrate to the cathode side as moisture provides the transport path (e.g. moisture absorbed by solder resist material). When the metal ions reach the cathode, dendritic growth can occur. Continuous reduction of dissolved metal ions leads to the nucleation and growth of metal dendrites, and eventually the formation of anode-cathode short failure [11]. The second kind of corrosion occurs in sub-surface associated with glass fibers/epoxy resin interface, so-called Conductive Anodic Filament (CAF) growth. The CAF grows from anode to cathode along delaminated fiber/epoxy interfaces when moisture is present. A CAF is made from soluble copper salt at anode and built at anode by turning to insoluble salt due to pH effect. Dendrite occurs as a result of solution at anode and plating at cathode.

In order to address those moisture effects, three kinds of accelerated moisture sensitivity/reliability tests are often applied for package reliability qualifications [2]. Moisture sensitivity test is required prior to reliability environmental stresses for all devices that are surface mounted to boards. Moisture/reflow sensitivity test has been documented in the joint JEDEC/IPC industry standard J-STD-020C [12]. This test specification has established exposure conditions of temperature, humidity, and time for which the moisture sensitivity rating of surface mount devices are classified and referenced. Moisture sensitivity levels (MSL) and the established test conditions for their measurement are shown in Table 1. Defined are six levels ranging from moisture insensitive (Level 1) to extremely sensitive (Level 6, bake from use). Moisture/reflow sensitivity test insures that the temperature, humidity and/or the shipping requirements are met before assessing the use reliability. The so-called Highly Accelerated Stress Test (HAST) (without electrical bias) is the second kind of the accelerated test to evaluate non-hermetic packaged devices in humid environments. The test employs temperature and humidity to accelerate the penetration of moisture through the external protective material or along the internal build-up or joined interfaces. Bias is not applied in this test to ensure the failure mechanisms potentially overshadowed by bias can be detected. This test is used to identify failure mechanisms internal to the package and is destructive. An autoclave test or steam test is similar to the HAST test. Steam test has a fixed temperature (121°C) and fixed RH (100%). During HAST, the packages are placed in the environmental chamber with humidity and temperature controls for certain period of time. Both steam and HAST remain standards based requirements. Lastly, the biased temperature/humidity (TH) test is a moisture test used to simulate the reliability of a powered device in an elevated temperature and high humidity environment under at nominal run state static bias (ranging from 0.1 to 7V). There are two standard forms of the biased moisture test that can be employed. The temperature, humidity bias (THB) test is performed at atmospheric pressure and temperatures between 30°C and 85°C and the relative humidity (RH) from 50% to 85%. The highly accelerated stress test with bias (HAST) is performed at less than 3 atmospheres of pressure and at temperatures between 110°C and 160°C.

Table 1 JEDEC specified moisture sensitivity level (MSL) and corresponding floor life

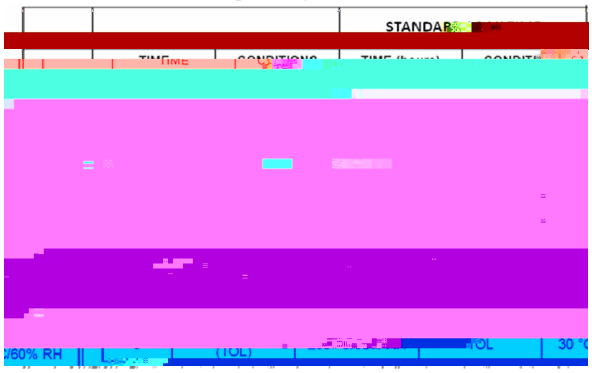


The most critical and contributory factor for most of moisture-induced failures is the adhesion degradation due to moisture, despite the failure mechanisms and testing conditions. For example, during surface mount process, interfacial delamination will occur due to the combinations of vapor pressure, thermal and hygroscopic stresses, but the package would remain intact if the adhesion strength is strong enough. During unbiased HAST, the resistance of adhesion strength to humidity/temperature aging is a key for the package integrity since significant hygroscopic stresses can be developed. For conductive anodic filament growth under biased HAST condition, the delamination/voids between the fiber/epoxy interface is responsible for the failure. Without defects or delamination, the CAF growth will not occur. Therefore, it is critical to characterize the adhesion strength of the interested interfaces as function of moisture, in particular, at elevated temperatures.

In this paper, several adhesion and fracture toughness characterization methods are introduced and applied to investigate the influence of moisture on interfacial fracture toughness or adhesion strength. Both interface fracture mechanics based fracture toughness measurement techniques and the quick-turn method such as die shear test are applied to investigate the interface behaviors with moisture. Details of experimental test setup, sample preparations and key results are presented. Next, the hygroscopic swelling measurement techniques are reviewed. Unfortunately, there is no standard hygroscopic swelling measurement method. The potential experimental errors associated with the TGA-TMA method are identified and studied analytically. A simple procedure for obtaining the coefficient of hygroscopic swelling is developed to eliminate the non-uniform moisture distribution effect. Both TGA-TMA method and Moiré interferometry method are applied to measure the hygroscopic swelling behaviors of several underfills. A methodology to allow a time-dependent finite element nonlinear analysis for package deformation and stress induced by hygroscopic as well as thermal mismatches is presented. The numerical results obtained from the integrated nonlinear finite element analysis are compared with the Moiré interferometry measurement. The effect of

hygroscopic swelling on the inter-layer dielectric integrity and under bump metallurgy (UBM) structures is investigated.

## 2. Influence of Moisture on Fracture Toughness/Adhesion Strength

It has been reported that the adhesion strength will be remarkably affected by moisture absorption [1,6, 13,14]. However, few reports are available where a systematic investigation of the measurement techniques for variations of interfacial fracture toughness with moisture has been carried out. In the following, both fracture mechanics based fracture toughness measurement techniques and the die shear test method were used to study the influence of moisture on fracture toughness/adhesion strength. The interface between polyimide on silicon chip and underfill (PI/UF) was used as a carrier in the following study.

### 2.1. In-situ fracture toughness measurement using double cantilever beam (DCB) specimen

A number of test specimens for investigating interfacial fracture energy have been developed over the years [15-17]. Few methods provide rigorous results which can be readily implemented on actual multilayer configurations. The particular difficulties in the measurement of interface fracture toughness are the sample preparation, and the design and implementation of test procedures that provide controlled, stable growth of the interface crack. Four-point bend test specimen has been successfully used in semiconductor industries to characterize the interfacial fracture toughness at silicon level with multi-stack layers of thin films. However, the fracture toughness at package level usually has higher fracture toughness (e.g. > 20 J/m$^2$ for PI/UF). Most often, when the interface strength is strong, the crack using 4-point bend specimen tends not to stay at the interface but goes into the silicon, rendering the interfacial fracture energy measurement meaningless. This has become a major issue when the test is performed in an environmental chamber for an in-situ measurement. In the following, the double cantilever beam (DCB) specimen structure was applied to measure the interfacial fracture toughness. The DCB silicon/underfill/silicon (Si/UF/Si) specimen preparation was shown in Fig. 1 in the following manner [18]. First, cut shims and dice Si wafers as the dimensions shown in Fig. 1. Apply PTFE type mold release agent to the bottom Si substrate, the applied area is 30 mm from the front edge. Place the top Si substrate, the shim, and the bottom Si substrate together as shown and fix them in place using two binder clips. Place the assembly on a hot plate set at certain temperature. Using a syringe, pump underfill material into the gap between the substrates from the rear end of the assembly and let the underfill material flow to the front end of the assembly by capillary action. Cure the underfill following the standard curing procedure. Cut the shim from the front edge and pull the shim out from the two sides of the assembly. Attach aluminum end-blocks to the top and bottom substrates using a room-temperature-cured epoxy. Aluminum end-blocks each with an extended arm were used to reinforce the silicon beam and prevent it from cracking during testing of Si/UF/Si samples, as shown in Fig. 2.

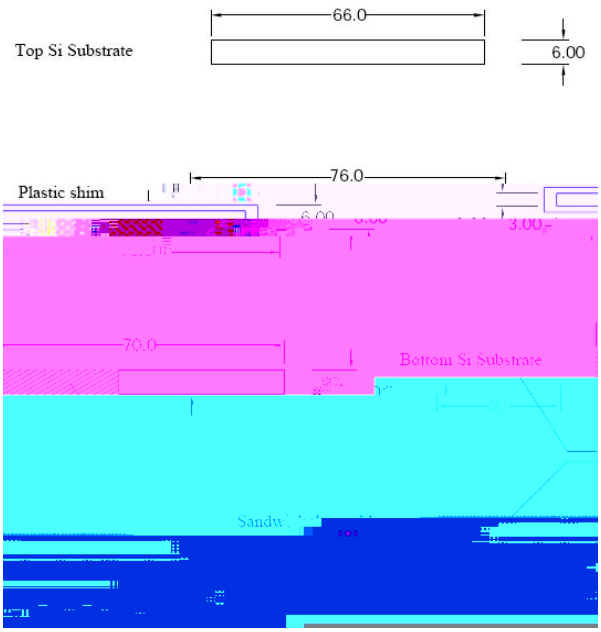


Fig. 1 Schematic of the assembly parts for a DCB Si/UF/Si sandwiching specimen

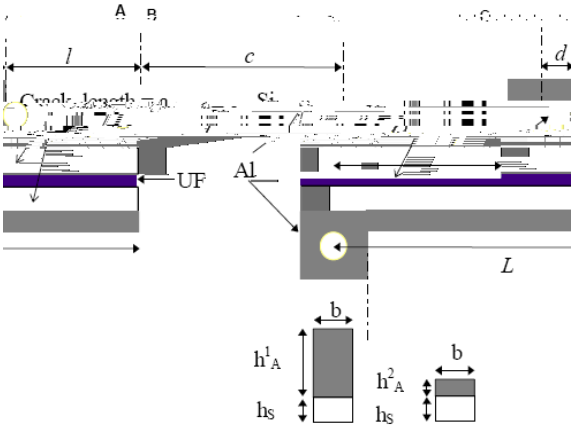


Fig. 2 Schematic of a Si/UF/Si sandwiching specimen for the DCB

Alternatively, the Si/UF/Si specimen can be prepared by dispensing the underfill before the top silicon part was placed (referred to 'open face' method). However, it has been shown that underfill filling by capillary force method shown in Fig. 1 resulted in much less scattered data for the interface fracture energy measurement than the 'open face' dispensation method [19]. This indicates that using capillary force dispensation method to prepare samples for DCB configuration is a critical process step ensuring good quality of interfaces under study. Such an assembly process also mimics the actual underfilling process.

The specimen was then placed in a humidity/temperature chamber attached to a mechanical tester for in-situ measurement. Typical load-displacement plots were shown in Figure 3 for a Si/UF/Si specimen. When the load-point displacement increased at a constant rate, the peak load was associated with the onset of the crack growth, and the load drop was associated with the crack jump/arrest. The load-

rising portion of each peak is nearly linear and can be used to determine the compliance and peak load needed for the analysis. After stable crack growth occurred (crack length increase from a to a+Δa), the displacement ramp was interrupted, the specimen was allowed to return to the original undeformed state and was re-loaded again with a constant displacement rate. Compliance C and peak load Pc were determined from each loading curve. The crack length was measured during the re-loading process when the interfaces in front of the crack tip were opened, and the crack tip was located via microscopy. It should be noted that in the beginning of a few cycles for loading and unloading, the data should be discarded because the pre-crack is not sharp enough and the initial stress-state of the system was not calibrated. When crack growth becomes substantially large, linear elastic fracture mechanics is not valid. Therefore, those data should be discarded too. Only the middle portion of the data shown in Fig. 3 was used to extract the fracture toughness. The details of fracture parameter extraction from the experimental data can be found in ref. [18].

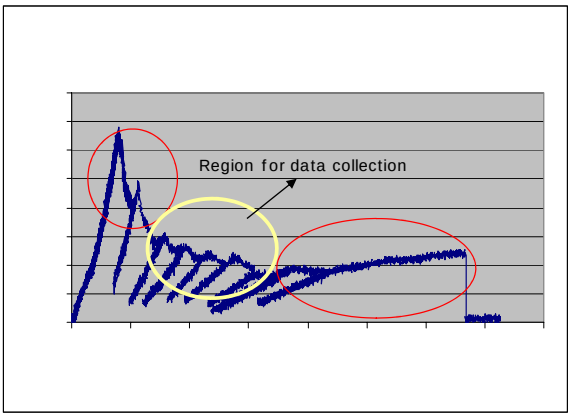


Fig. 3 Typical loading-unloading curve for a Si/UF/Si DCB specimen

Fig. 4 plotted the test results in three different conditions. The 'case 2' represented the fracture toughness at room condition after the sample was assembled. A significant difference was observed for the fracture toughness at room condition and the one after 1 hour bake at 130°C. This was possibly due to the moisture effect at room condition, in which a ~30%RH was expected. Since the underfill was cured following exact the curing schedule, the suspicion of whether or not the undefill was fully cured was eliminated. As expected, the fracture toughness decreases after moisture preconditioning at 85°C/85%RH for 5 days, as shown in Fig. 4.

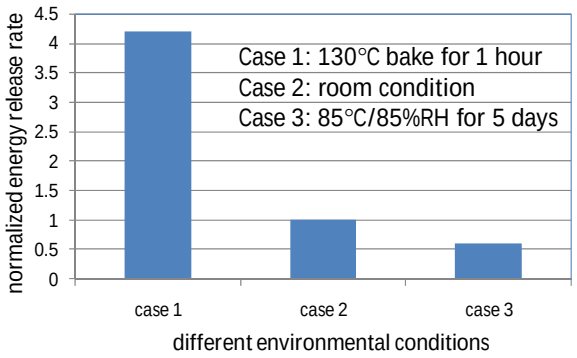


Fig. 4 Fracture toughness for a Si/UF/Si assembly under different environmental conditions

### 2.2 Fracture toughness measurement using photomechanics measurement techniques

An integrated multi-functional micro-moiré interferometry ($M^3I$) system, which combines moiré interferometry (MI) technique with thermoelectric heating and cooling, humidity system, and microscopic imaging system [20], was applied to obtain the deformation field to extract the fracture parameters. A miniaturized moisture chamber with ultrasonic humidity excitation was developed to control the hygrothermal conditions within the error of 0.1°C and 1%RH. Micro-digital image speckle correlation (μ-DiSC) was also applied to obtain the fracture toughness of investigated samples. In this study, silicon/underfill/FR-4 assemblies were prepared as shown in Fig.5. The attention was drawn on the interfacial delamination behavior between silicon/underfill. The assembly consisted of three materials, namely, silicon, underfill and FR-4. The dimensions of the assembly were 8 mm(L)x5 mm(W) x1.8 mm(H). The thickness of the underfill was 0.5 mm. A pre-crack was prepared at the silicon/underfill interface by using a piece of silicon rubber film with thickness of 20 μm. The length and the ligament of ahead of the crack tip were respectively 2.7 mm and 5.3 mm, respectively. The selection of these dimensions was to neglect edge effects on loading. A dispenser and a curing oven were employed to prepare the assembly. By the capillary effect, underfill was dispensed into the gap between the silicon and FR-4. When the specimen was partially cured, the rubber was quickly removed from the specimen and a sharp crack was fabricated. After fabrication, each assembly was carefully polished with a fine SiC paper to remove excessive underfill and to obtain the desired dimensions. Specimen grating with a frequency of 1200 lines/mm was replicated onto the surface of the assembly at room temperature. The assembly was then put into the miniaturized moisture chamber with the hygrothermal loading conditioned at 85°C/85%RH for 168 hours. The moiré fringe patterns were captured at the times of 0, 1, 3, 7, 11, 24, 48, 96 and 168 hour. In order to eliminate the time and thermal effect, i.e. creep of underfill material, a parallel test on the same sample without moisture absorption was carried out and the moiré fringe patterns were acquired at the same time intervals.

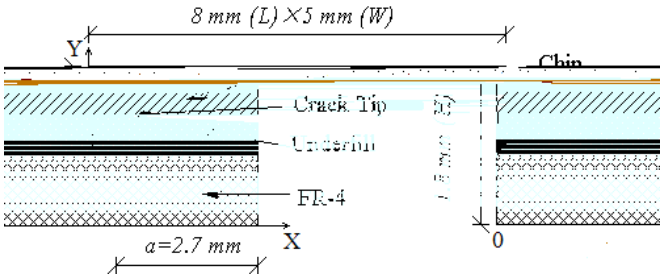


Fig. 5 Schematic diagram of the silicon/underfill/FR-4 assembly

The DIC technique was combined with a sandwiched brazil-nit (SBN) fixture for the characterization of the critical interfacial fracture toughness of silicon/underfill interface under different mixed-mode loading conditions [20]. The sandwich structure was made of silicon/underfill/silicon with a 4mm pre-crack manufactured at the silicon/underfill interface. The thickness of the underfill was chosen to be 0.5 mm, which is consistent with the thickness in the moiré experiment. The SBNs were aged under 85°C/85%RH in a hygrothermal chamber for 168 hours beforehand. Artificial speckle patterns were subsequently generated on the specimen surface using white paint and carbon particles to create images with high contrast of gray level. The interfacial fracture tests on the samples were conducted with INSTRON micro-tensile machine at room temperature. A high resolution CCD camera was used to capture speckle patterns at different load levels. With the curve, the speckle pattern at the load level where the interface crack opened could be obtained. This pattern and the initial speckle pattern were used as undeformed and deformed images. With the correlation software, the displacement fields around the crack-tip could be determined.

Fig.6 plotted the mode I and Mode II stress intensity factors at different hygrothermal aging times based on the moiré fringe measurement. It can be observed that the hygroscopic stresses increase with the time of moisture absorption, therefore the stress intensity factors increase with time. Then the stress intensity factors level off to reach an asymptotic value, which indicates that the assembly is saturated with moisture absorption. The asymptotic curve suggested that the change of the fracture behavior induced by moisture absorption was gradual rather than instant, although the in-plane surface measured was in the boundary condition of saturated moisture concentration. It should be noted that the results plotted in Fig.6 were combined effect with hygroscopic stresses and thermal stresses. In order to eliminate the thermal effect, dried sample was tested in the same way, as plotted in Fig. 7. Both $K_1$ and $K_2$ started to decrease with time due to the creep behavior of underfill for dry samples. The assembly was complexly relaxed after the certain period of time. Time effect was significant in the hygrothermal aging, especially at the high temperature. In addition, it can be seen that the magnitude of stresses or fracture parameters on time effect was comparable to that on hygrothermal induced swelling. Therefore, the results indicated that the interface toughness induced by the moisture swelling was possible to be overestimated if the time effect was not considered.

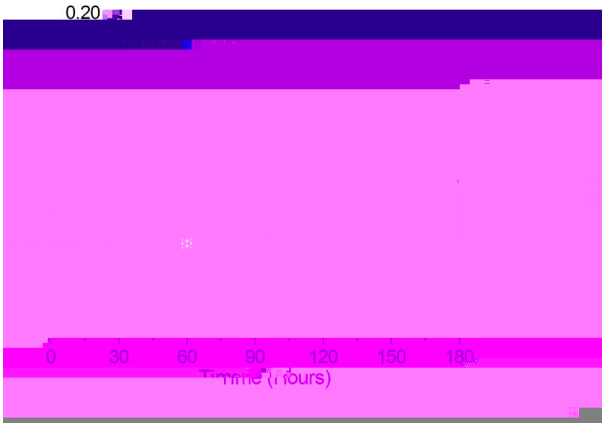


Fig. 6 $K_1$ and $K_2$ with respect to different hygrothermal aging time (85 ºC/85%RH)

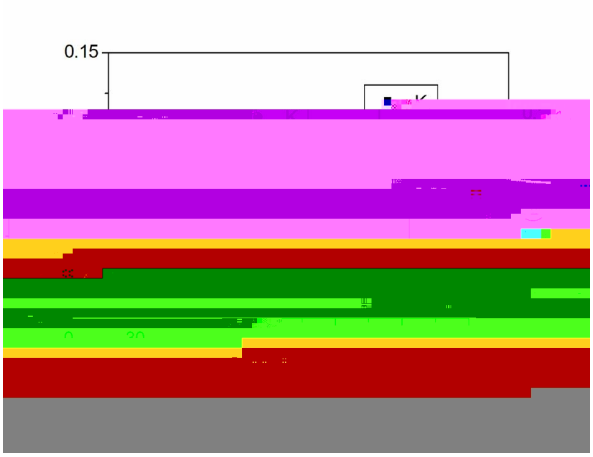


Fig. 7 $K_1$ and $K_2$ with respect to different thermal aging time (85 ºC)

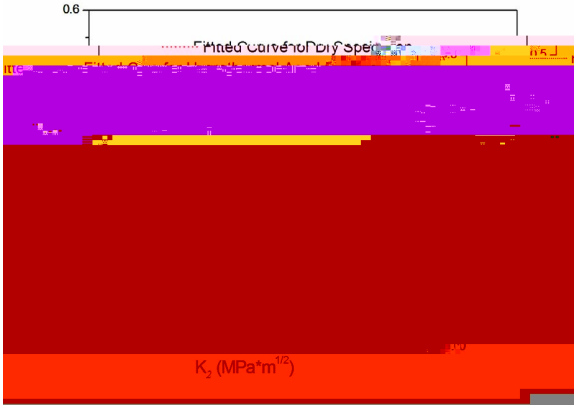


Fig. 8 Fracture toughness of dry and wet (85°C/85%) SBN specimen

Based on the μ-DiSC system and interface fracture mechanics, the measured results of fracture toughness in terms of $K_{1C}$ and $K_{2C}$ were presented in Fig.8. It can be seen the critical interfacial fracture toughness $K_{1C}$ and $K_{2C}$ followed the ellipse law with respect to different phase angles.

By varying the loading angles, different mode mixities were achieved. However, the $K_{1C}$ decreased slowly when $K_{2C}$ increased by changing the loading angle from 90° to 20°. This indicated that the $K_{1C}$ plays a more critical role in the determination of critical interfacial fracture toughness than $K_{2C}$. After the hygrothermal aging, the critical interfacial fracture toughness decreased significantly compared with the critical interfacial fracture toughness of dry specimen tested at the room temperature. After 168 hours of exposure at 85 °C/85%RH, the interfacial adhesion was decreased on average 34.9% for the silicon/underfill interface. This is because that the moisture could invade into the defects and remarkably decrease the interfacial strength by intercepting the inter- and intra-molecular hydrogen bonding provided by the hydroxyl groups.

### 2.3 Die shear test

Although interfacial fracture mechanics based fracture toughness measurement provides rigorous definition and results for evaluating interface strength, the sample preparation is very tedious, and the procedure often is not compatible with packaging assembly process. On the other hand, die shear test, by which the samples can be made by standard packaging and assembly processes, provides an effective way for a quick assessment of the adhesion strength. A new method for sample preparation is introduced in the following to generate a large quantity of samples. The interface between polyimide on silicon chip and underfill were evaluated. The silicon chip on silicon substrate configuration was designed to eliminate the thermo-mechanical stresses due to CTE mismatch. Such a configuration has two identical interfaces on both sides so that the fracture mode can be controlled better. Fig. 9 showed the schematic of sample preparation process. It started from a silicon wafer with PI psssivation. A stencil was designed and applied to control the area and height of underfill dispensation. A flip-chip pick and place machine was used to assemble 2x2 mm silicon dies on the wafer. The whole assembly was then cured according to each underfill's prescribed curing schedule. Specimens were ready for the test after dicing. Such a sample preparation process could produce a large quantity of specimens and minimize the sample-to-sample variations. All specimens have consistent wetting area and location and underfill height. Die shear tests were performed on a die shear tester system: DAGE Series 4000 with hot plate (temperature range 25°C - 300°C). The system has a fixed hot plate and test table with full automatic test process. Several parameters such as shear speed and shear height can be adjusted to control the fracture mode. In the present study, the shear height was set equal to the underfill height and shear speed was set as 200μm/s. For all experimental legs shown later, the sample size was 16 units per leg. 100% failure along the interface was achieved for all legs. The standard deviation of the measured adhesion data were less than 15%.

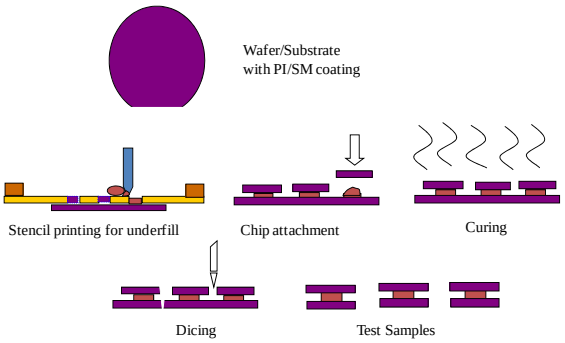


Fig. 9 Schematic of die shear test specimen preparation process

Our particular interest was to evaluate the adhesion strengths for three types of underfill under various moisture/temperature conditions. First, the moisture absorption characteristics were obtained for these three underfills by moisture weight gain experiment. Table 2 summarized the diffusivity and the saturated moisture concentration at 85°C/85%RH. Then the moisture diffusion modeling was conducted to understand the soak time requirement. Since silicon chips on the both sides of the specimen do not absorb moisture, the moisture is diffused through the underfill only from underfill side. According to the moisture modeling results, it takes more than three weeks for the sample fully saturated 85°C/85%RH. Two experimental plans were defined. In the first group, the objective was to compare the adhesion strength at room temperature under different soaking conditions. Table 3 listed the details of the experimental legs for the first group. The second group was designed to obtain the adhesion strength at 220°C with moisture, as shown in Table 4. In order to measure the adhesion strength at 220°C, the preconditioned samples were placed to the hot plate immediately right after removed from the humidity chamber. Since this is not an in-situ measurement, moisture will be escaped during the heating process. However, the majority of moisture at PI/UF interface remained intact. Such a process could simulate the real reflow process for a package, in which moisture loss is expected during reflow.

Table 2 Moisture diffusivity and saturated moisture concentration at 85°C/85%RH for three underfills

| Material | Diffusivity | Csat |
|---|---|---|
| | cm^2/s | g/cm^3 |
| UF1 | 1.509E-08 | 1.717E-02 |
| UF2 | 2.441E-09 | 2.430E-02 |
| UF3 | 2.675E-09 | 1.713E-02 |

Table 3 Experimental legs for three underfills at room temperature under different moisture conditions

| | | | | |
|---|---|---|---|---|
| | | | | |
| | | | | |
| | | | | |
| | | | | |
| | | | | |

Table 4 Experimental legs adhesion measurement at 220C° for three underifills under different moisture conditions

| | | | | |
|---|---|---|---|---|
| | | | | |
| | | | | |
| | | | | |
| | | | | |
| | | | | |

Fig. 10 plotted the adhesion results at room temperature for three different underfills under various soaking conditions. It showed that the differences in adhesion among the three underfills at room temperature are not significant. It is also noted that the adhesions for these three underfills are not sensitive to moisture at room temperature.

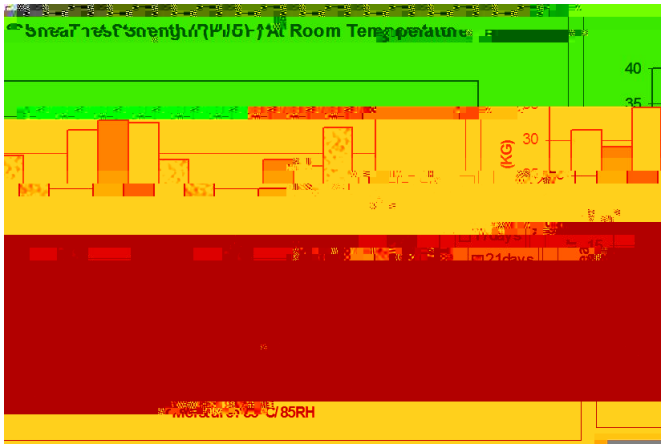


Fig. 10 adhesion strength at room temperatures under different moisture conditions for three underfills

Fig. 11 plotted the test results for these three underfills at 220°C under various conditions. It clearly shows that the moisture has strong influence on the adhesion strength at elevated temperature. This implies that the adhesion test at high temperature is necessary for the correlation with the actual material performance during moisture sensitivity test [1,6]. Compared to the moisture absorption data in Table 2, there was no correlation for the adhesion with the saturated moisture concentration and diffusivity. For a particular material, even though material is able to absorb more moisture than other materials, the delamination may not be a concern if the adhesion at the interface of interest after moisture absorption at high temperature is strong enough [6]. The adhesion at room temperature may not be able to represent the interface behavior. Only the adhesion measurement at elevated temperature with moisture effect correlates with the reflow performance.

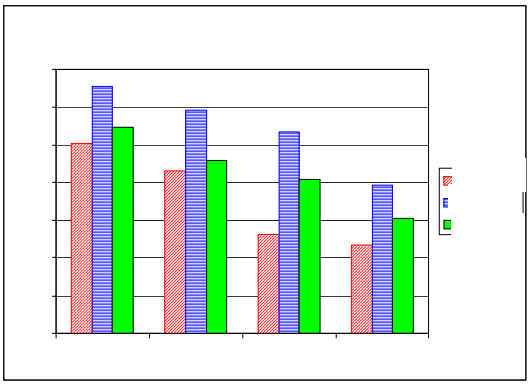

Fig. 11 adhesion strength at 220°C under different moisture conditions for three underfills

## 3 Hygroscopic Swelling Characterization and Analysis

Hygroscopic stresses arise in an electronic package when the polymeric materials swell upon absorbing moisture while the adjacent nonpolymeric materials, such as silicon chip, do not experience swelling. The differential swelling leads to hygroscopic mismatch stresses in the package. Swelling measurements can be made by the use of many different experimental techniques [20-23]. However, there have been no standard-based procedures for hygroscopic swelling measurements. A thermo-mechanical analyzer (TMA), which uses a deformation probe, has been used to measure length changes in the sample due to moisture loss at a constant temperature. The resolution of the TMA length measurement is usually 0.0001 mm or smaller. In each test, a thermo-gravimetric analyzer (TGA) is also used to measure the in-situ weight loss for an identical sample with identical temperature ramp rate used in TMA. In this combined TGA-TMA technique, the samples are preconditioned until saturation before placed into TMA and TGA chambers. During the measurements, desorption takes place. The dimensional change (average strain) and weight loss (averaged moisture concentration) can be recorded simultaneously. Fig. 12 showed the schematic of TGA-TMA method, and Fig. 13 showed a typical plot for averaged strain versus averaged moisture concentration based on the TGA-TMA measurement data.

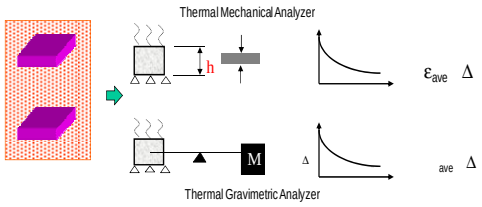


Fig. 12 TGA-TMA hygroscopic swelling measurement setup

In order to describe the swelling behavior, the coefficient of hygroscopic swelling (CHS) has been defined as follows

$$\varepsilon = \beta C \qquad (1)$$

where $\varepsilon$ and $C$ are the hygroscopic strain and moisture concentration, respectively, and $\beta$ is the coefficient of hygroscopic swelling of the material. The coefficient $\beta$ was

determined by a linear curve fit method through the plot shown in Fig. 13, i.e, the slope of the linear fit.

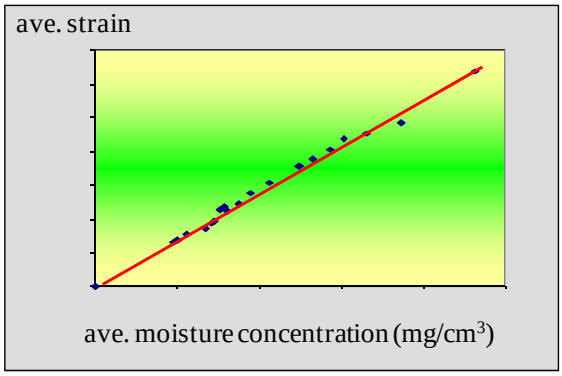


Fig. 13 A tyical avergae strain/average moisture concent plot from TMA-TGA desorption test

Two potential sources of errors have been identified and investigated in the above swelling measurement and analysis [24-26]: one was due to the effect of defining the averaged strain and the averaged moisture concentration, and the other was the effect of non-uniform moisture distribution during TGA-TMA measurement. Although a linear regression is usually well achieved as shown in Fig. 13, the hidden errors could lead to incorrect material characterization.

There are two averaged methods in order to obtain a plot shown in Fig. 13. In the method I, the averaged strain and moisture concentration can be defined and calculated with respect to dry conditions. In this case, we have

$$\varepsilon_{ave}^{I} = \frac{h(t) - h_x}{h_x} = \frac{\Delta h_x(t)}{h_x} \tag{2}$$

$$C_{ave}^{I} = \frac{M(t) - M_0}{V_0} = \frac{M_{\text{moisture}}(t)}{V_0} \tag{3}$$

where, the average strain is defined with regard to the reference point in dry conditions. $M(t)$ is the total weight of specimen and $M_0$ is the specimen weight in dry condition. $M_{\text{moisture}}(t)$ is the moisture weight at time $t$, and $V_0$ is the initial specimen volume, i.e.,

$$V_0 = h_x h_y h_z\big|_{\text{dry}} \tag{4}$$

in which, $h_x$, $h_y$, and $h_z$ are lengths of the plate in three directions respectively. The superscript $I$ denote the averaged method with respect to dry conditions. The averaged coefficient of hygroscopic swelling can then be obtained by

$$\varepsilon_{ave}^{I} = \beta_{ave}^{I} C_{ave}^{I} \tag{5}$$

or

$$\beta_{ave}^{I} = \frac{\varepsilon_{ave}^{I}}{C_{ave}^{I}} \quad . \tag{6}$$

Alternatively, in method II, the average strain and moisture concentration can be defined as follows, respectively,

$$\varepsilon_{ave}^{II} = \frac{h_{sat} - h(t)}{h_{sat}} \tag{7}$$

$$C_{ave}^{II} = \frac{M_{sat} - M(t)}{V_0} \tag{8}$$

in which, the average strain is defined and calculated with regard to the reference point in fully saturated conditions. $h_{\text{sat}}$ and $M_{\text{sat}}$ are the thickness and the moisture mass of specimen at time zero when the specimen is fully saturated.

Similarily, the averaged coefficient of hygroscopic swelling can be obtained by

$$\beta_{ave}^{II} = \frac{\varepsilon_{ave}^{II}}{C_{ave}^{II}} \tag{9}$$

Now, the effect of non-uniform moisture distribution is considered. Assume that the true hygroscopic swelling coefficient is β, and then the ratio $R^I$ and $R^{II}$ can be defined as below,

$$R^I = \frac{\beta_{ave}^{I}}{\beta} \tag{10}$$

$$R^{II} = \frac{\beta_{ave}^{II}}{\beta} \tag{11}$$

Three-dimensional moisture diffusion solution was employed to consider the non-uniform moisture distribution. The analytical expressions of both averaged methods were obtained as follows,

$$R^I = \frac{\beta_{ave}^{I}}{\beta} = \frac{\frac{\pi^2}{4}\sum_{n=0}^{\infty}\frac{(-1)^n}{(2n+1)}\exp\left(-\frac{Dt}{h_y^2}(2n+1)^2\pi^2\right)\sum_{n=0}^{\infty}\frac{(-1)^n}{(2n+1)}\exp\left(-\frac{Dt}{h_z^2}(2n+1)^2\pi^2\right)}{\sum_{n=0}^{\infty}\frac{1}{(2n+1)^2}\exp\left(-\frac{Dt}{h_y^2}(2n+1)^2\pi^2\right)\sum_{n=0}^{\infty}\frac{1}{(2n+1)^2}\exp\left(-\frac{Dt}{h_z^2}(2n+1)^2\pi^2\right)} \tag{12}$$

$$R^{II} = \frac{\beta_{ave}^{II}}{\beta} = \frac{1 - \frac{128}{\pi^4}\sum_{n=0}^{\infty}\frac{(-1)^n}{(2n+1)}\exp\left(\frac{Dt}{h_y^2}(2n+1)^2\pi^2\right)\sum_{n=0}^{\infty}\frac{(-1)^n}{(2n+1)}\exp\left(\frac{Dt}{h_z^2}(2n+1)^2\pi^2\right)\sum_{n=0}^{\infty}\frac{1}{(2n+1)^2}\exp\left(\frac{Dt}{h_x^2}(2n+1)^2\pi^2\right)}{1 - \frac{512}{\pi^6}\sum_{n=0}^{\infty}\frac{1}{(2n+1)^2}\exp\left(\frac{Dt}{h_y^2}(2n+1)^2\pi^2\right)\sum_{n=0}^{\infty}\frac{1}{(2n+1)^2}\exp\left(\frac{Dt}{h_z^2}(2n+1)^2\pi^2\right)\sum_{n=0}^{\infty}\frac{1}{(2n+1)^2}\exp\left(\frac{Dt}{h_x^2}(2n+1)^2\pi^2\right)} \tag{13}$$

where the plate specimen possesses finite length in three dimensions as $h_x$, $h_y$, and $h_z$, D is the moisture diffusivity ($mm^2/s$), and t is the time (s). Equations (12) and (13) established the relationships of errors ($R^I$ and $R^{II}$) as function of specimen diemasions, material dissusivity and measurment t). It showed that

$$\frac{\pi^2}{4} \geq R^I = \frac{\beta_{ave}^{I}}{\beta} \geq 1 \tag{14}$$

$$1 \geq R^{II} = \frac{\beta_{ave}^{II}}{\beta} \geq 0.267 \qquad (15)$$

or

$$(t \to \infty) \quad 2.46\beta \geq \beta_{ave}^{I} \geq \beta \quad (t \to 0) \qquad (16)$$

$$(t \to \infty) \quad \beta \geq \beta_{ave}^{II} \geq 0.267\beta \quad (t \to 0) \qquad (17)$$

The above results imply that the potential error with the TGA-TMA method could overestimate the CHS as much as 246% if the averaged method uses dry condition as reference condition, while the CHS could be underestimated as much as 27% if the averaged method uses fully saturated point as reference condition.

Equations (16) and (17) also inferred how to select the data points to obtain the CHS accurately. When the averaged method I is used, the experimental data should be taken for the period in the beginning of desorption. As shown in Equation (16), the averaged CHS will be closer to the true CHS when t approaches 0. When the averaged method II is used, the data should be collected after a long period of desorption. These two methods give the upper and lower bound estimates of the coefficient of hygroscopic swelling of materials. It is obvious that the non-uniform moisture distribution during desorption could introduce the errors in the coefficient of hygroscopic swelling. A general procedure in determining the accurate coefficient of hygroscopic swelling has been be suggested as following,

1. Bake the specimen until it is absolutely dry;
2. Let the specimen absorb moisture at certain temperature and certain relative humidity until full saturation;
3. Measure the length $h_{sat}$ and weight $M_{sat}$ of specimen initially and keep the probe the same location;
4. Let the sample dry out completely and record the length $h_x$ and weight $M$ of specimen, which represent the values at dry conditions, denoted by $h_0$ and $M_0$ respectively.

The coefficient of hygroscopic swelling $\beta$ is then calculated by

$$\beta = \frac{(h_{sat} - h_0)/h_0}{(M - M_0)/(h_{x0}h_{y0}h_{z0})} \qquad (18)$$

The coefficient of hygroscopic swelling determined in this way is easier and accurate, and it can eliminate the effect of non-uniform moisture distribution. The errors caused by selecting the data sets in certain time range for the linear regression can also be avoided.

Moiré interferometry is another method reported in the literature to measure the hygroscopic swelling [20-21]. Moiré interferometry measures in-plane displacements with very high sensitivity. It has been practiced extensively in the microelectronics industry to measure the thermally induced deformation of electronic packages. For hygroscopic swelling measurements, it is vital to eliminate thermal expansion during moiré measurements so that only hygroscopic swelling is documented. This was accomplished by using the reference sample. The reference and test samples were positioned side by side within the viewing area of the moiré setup. This procedure canceled any thermally induced deformations in the test sample since the deformed state of the reference sample was used as a reference datum for zero hygroscopic deformation of the test sample.

Both the TGA-TMA method and Moiré interferometry method were applied to characterize the hygroscopic swelling of three underfills. Table 5 gave the results comparison based on the traditional linear regression method and the simple procedure suggested above. It indeed showed that the traditional slope method overestimated the CHS significantly. Further, the Moiré interferometry method was used to validate the simple procedure using TGA-TMA method, and excellent agreement was obtained, as shown in Table 6.

Table 5 Comparison of the CHS based on the traditional slope method and new procedure

| | | | |
|---|---|---|---|
| | 1 | | |
| | | | |
| | | | |

Table 6 Comparison between TGA-TMA method and Moiré interferometry method

| Method | CHS |
|---|---|
| TMA-TGA with new procedure | 0.21 |
| Moiré interferometry | 0.20 |

The experimental raw data from TGA-TMA test was analyzed using the above analysis as described by equations (12) and (13). The theoretical predictions and experimental data were presented in Fig. 14. It can be seen that the theory corroborated with the experimental results very well. More experimental fluctuations were observed for experimental results obtained based on the averaged method 1. Overall two averaged approaches presented upper and lower bound of the true value of coefficient of hygroscopic swelling.

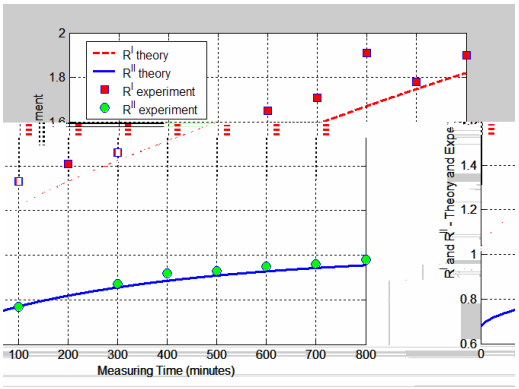


Fig. 14 Experiment versus theory for $R^I$ and $R^{II}$ as function of time

It has been suggested that swelling is caused by water molecules bound to the polymer matrix and not by the free water molecules [3]. Because the water molecule is polar, it is capable of forming hydrogen bonds with hydroxyl groups, thereby disrupting inter-chain hydrogen bonding with the net effect of increasing the inter-segmental hydrogen bond length. It reveals that the volume change by hygroscopic swelling is only a small fraction of the total free volume. The formation of hydorgen bond with polymer materials causes the hygroscopic swelling of material, while the unbound water liquid/vapor fills in free volumes, which does not cause swelling if the vapor pressure is low at lower temperatures. Therefore, the equation (1) might needs to be modified if only a small fraction of moisture is responsible for the swelling of material. Instead of using the total moisture concentration in equation (1), the moisture concentration fraction which forms the hygro bonding may be used.

$$\varepsilon_{\text{swelling}} = \beta C^{\text{bound water}} \tag{19}$$

where $C^{\text{bound water}}$ is the moisture mass for the bond formation per unit volume.

## 4. Coupled Nonlinear Thermal-Hygro-Stress Modeling

The integrated stress modeling under temperature/humidity loading condition requires five types of modeling, i.e., moisture diffusion during moisture preconditioning and reflow, thermal modeling, hygro-mechanical modeling, thermo-mechanical modeling, and vapor pressure modeling [27-30]. This is a coupled field multi-physics problem that involves with thermal analysis, moisture diffusion, moisture phase change, and nonlinear stress analysis. There are extensive studies in literature on thermal-hygro stress modeling. However, most of the published work uses linear elastic analysis to simplify the problem. So the superposition method, in which an equivalent coefficient of thermal expansion is introduced, can be applied. For example, if $\varepsilon_T$ is thermal strain, $\alpha$ the coefficient of thermal expansion, and $\Delta T$ is the change of temperature, then the thermal strain can be written as

$$\varepsilon_T = \alpha \Delta T, \tag{20}$$

Similarly,

$$\varepsilon_h = \beta C \tag{21}$$

where $\varepsilon_h$ is the hygroscopic swelling strain, and $C$ represents the moisture concentration. When an electronic package is applied to both thermal and hygroscopic loadings, the total expansion strain is

$$\varepsilon = \alpha \Delta T + \beta C \tag{22}$$

Consider a special case, where the temperature and moisture across a material in the package are uniform (the moisture concentration is not necessarily uniform across the whole package). When linear elastic analysis is assumed, the hygroscopic strain can be treated as additional thermal strain. Thus, an equivalent coefficient of thermal expansion $\alpha^*$ can be defined as follows

$$\alpha^* = \alpha + \beta C / \Delta T, \tag{23}$$

then

$$\varepsilon = \alpha^* \Delta T \tag{24}$$

Equation (24) indicates that the equivalent coefficient of thermal expansion $\alpha^*$ instead of $\alpha$ can be used to conduct an integrated thermal and hygroscopic stress analyses using the conventional thermal stress analysis method.

As presented previously in Figs. 6 and 7, when the effect of thermal aging due to the viscoelastic behavior of underfill is considered, a simple superposition of hygro-and thermal strains is not valid anymore. Time-dependency and nonlinear behavior of materials must be considered. Unfortunately, commonly used commercial finite element software such as ABAQUS and ANSYS do not explicitly allow the fully coupled time-dependent thermal and hygroscopic nonlinear stress analysis.

In the following, a multi-step temperature/humidity loading profile is considered, as shown in Fig. 15. Such a loading profile represents a typical loading condition that starts from packaging assembly process and then move to HAST stress condition. Moisture loading is applied at Step 4 when the package is placed into a HAST chamber, where transient moisture diffusion and hygroscopic swelling takes place at a constant temperature. The objective is to determine the package deformation and stress buildup history with respect to time during HAST. The nonlinear and temperature-dependent material behavior such as underfill and solder material needs to be considered. The transient moisture diffusion during HAST should be incorporated.

Careful examination of the loading profile shown in Fig.15 reveals that the temperature loading can be decoupled from moisture loading in each loading step. In Steps 1 to 3, moisture is not present, therefore, a conventional nonlinear multi-process stress modeling methodology can be applied with the help of element death and birth and multi-constraint functions if necessary [31]. At step 4, the package is exposed to a moisture loading condition at a constant temperature. Since the heat conduction is much faster than moisture diffusion during HAST, it is reasonable to assume the isothermal condition at Step 4. The transient moisture diffusion and the subsequent hygro-stress modeling can be performed using the coupled thermal stress analysis provided in the software. It is noted that the built-in temperature field in the software at this step is replaced by the transient moisture field analysis so that the nonlinear hygrostress analysis can be carried out. An additional field variable should be defined (in ABAQUS keyword *FIELD), which represents the temperature field. The stress state carried over from the previous loading step is considered as initial stresses, and the material properties at Step 4 can be updated with the material properties with moisture effect. At Step 5, when the package is removed from the HAST chamber and ramped down to the room temperature, the moisture loss during Step 5 is not significant, therefore, moisture diffusion is not considered. The built-in temperature field is now ‘switched’ back to represent the temperature field to conduct the conventional non-linear stress analysis. Step 6 is similar to Step 4 with transient moisture desorption occurring and the stress state at the end of previous step is the initial stress state.

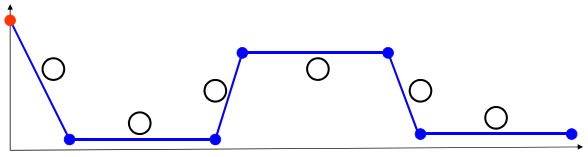

Fig. 15 a typical multi-step temperature/humidity loading profile

The above modeling approach was applied to a flip chip package subjected to a loading profile defined in Fig. 15. The moiré measurement was also applied to measure the deformation history during HAST at Step 4. The moiré system was tuned at the grating replication temperature 85°C. The package was then subjected to 85°C /85%RH. Fig. 16 showed the comparison between the finite element analysis and the moiré measurement. It is noted that the fringe patterns represent the hygroscopic mismatch deformation only and do not contain any thermally induced deformations. Fig. 17 showed the moisture diffusion history and the progressive hygroscopic swelling induced package deformation.

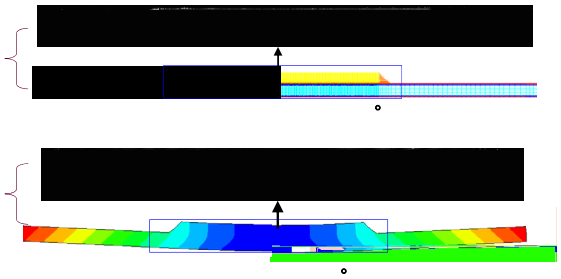

Fig. 16 Comparison between moiré measurement and finite element analysis

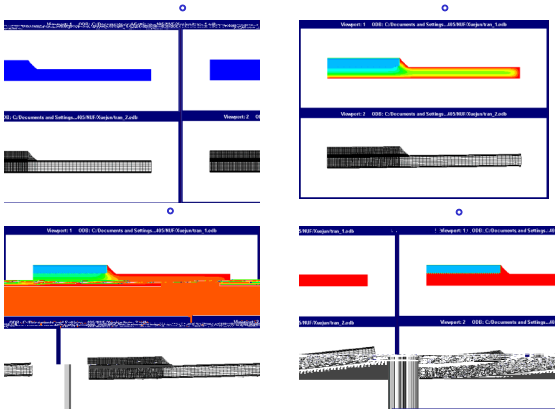

Fig. 17 Moisture diffusion and package deformation history during HAST

The particular interest is the stress pattern and distribution of under bump region along the chip surface, which represents the packaging stresses exerted on the inter-layer dielectric (ILD) and under bump metallurgy (UBM) structure, or ILD/UBM, structures. A global-local modeling scheme was applied. Fig. 18 showed the bump region structure and local finite element mesh patterns.

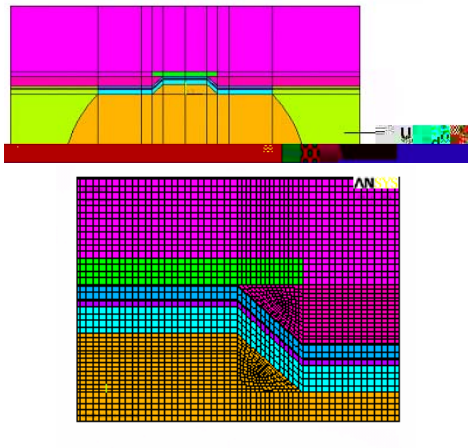

Fig. 18 local finite element model of the inter-layer dielectric (ILD) and under bump metallurgy (UBM) structure, or ILD/UBM, structures

Figures 19 plotted the maximum normal stress and shear stress at the end of the Step 4. The stresses were taken from a point along the under chip surface of ILD/UBM structure. Along the UBM or die/bump interface, hygroscopic swelling induces tension while thermal loading itself causes compression. Normal stress due to hygroscopic stress is twice as high as the value of thermal stress. Shear stress due to hygroscopic swelling also increases. FEA simulation results reveal the significance of contribution of hygroscopic swelling induced tensile stresses under bump region. Since in general the HAST temperature is lower than the curing temperature, locally thermal strain due to the thermal mismatch between bump and underfill is compressive, therefore, applies the compressive stresses on the under bump and die surface. During HAST, with more moisture absorbed, the underfill and substrate swell to cause the hygroscopic swelling stresses. These stresses are tensile state under bump, which causes ILD/UBM opening failure. Both tensile stress and shear stress reach their highest value near the upper corner of bump, from where the package failure usually initiates [32]. Both hygroscopic swelling induced tensile and shear stresses impose a potential threat to ILD/UBM failure.

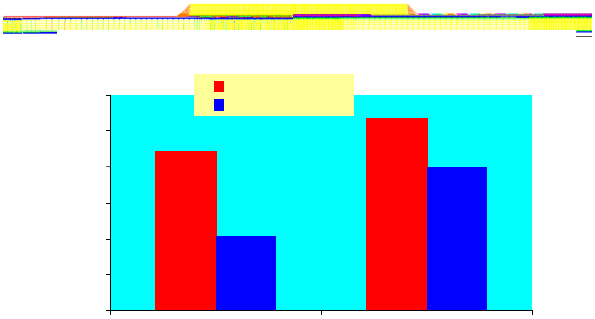

Fig. 19 maximum normal and shear stress at UBM/ILD region in a flip chip package

## 5. Conclusions

The influence of moisture on interface fracture toughness or adhesion strength is a key for package intergrity and reliability in spite of failure mechanisms and environmental

conditions. Sample preparation and, the implementation and design of test procedures for adhesion measurement are critical to ensure a controlled and stable grwoth of interface crack, from which the interfcae material properties can be obtained. This paper details several methods in sample preparations. Both fracture mechanics based interface fracture toughness measurement techniques and adhesion measurement using die shear test were applied to investigate the material interface properties. It has been found that adhesion test at high temperature is necessary for the correlation with the actual material performance during moisture sensitivity test. The adhesion at room temperature may not be able to fully represent the interface behavior at higher temperature. Only the adhesion measurement at elevated temperature with moisture effect correlates with the reflow performance.

Both TGA-TMA method and Moiré interferometry wee applied to characterize the hygroscopic swelling of underfill materials. The potential source of error that is associated with the TGA-TMA method is due to the non-uniform moisture distribution. The analytical results showed that the TGA-TMA method could overestimate the CHS as much as 246% if the averaged method uses dry condition as reference condition, while the CHS could be underestimated as much as 27% if the averaged method uses fully saturated point as reference condition. In order to obtain the true property of swelling, a simple procedure has been suggested, in which only two points are taken: one point with fully saturated condition, and another point with fully dry condition. Those two points satisfy the uniform moisture distribution requirement. Excellent agreement has been reached for the hygroscopic swelling characterization by both TGA-TMA method and Moiré interferometry methods, when the non-uniform moisture distribution effect is removed.

A new finite element analysis methodology is presented in this paper, by which, the time-dependent nonlinear analysis of package deformations induced by hygroscopic as well as thermal mismatches can be analyzed. The existing linear superposition method, which couples hygroscopic stress with thermal stress analysis, can not apply to the problem with the nonlinear material properties. The proposed method allows a fully integrated nonlinear finite element stress modeling during HAST to capture the time-dependent deformation and stress buildup. The Moiré interferometry measurement was then applied to a high-density flip chip package to measure the warpage and the strains of package. The numerical results by nonlinear finite element analysis had very good agreement with the experimental data. The results of the effect of hygroscopic swelling on the inter-layer dielectric reveals that the overall ILD stresses under HAST can be twice as high as those considered without the moisture effect.

**Acknowledgments**

This paper touches upon quite a number of research areas, and represents the collected contributions of several individuals, institutions and companies. Albeit incomplete, I'd like to note the following key individuals/mentors and their respective organizations:Tong Yan Tee (Amkor), Steve Cho (Intel), Yi He (Intel), Xuefeng Zhang (University of Texas at Austin), Daniel Shi (ASTRI), Zhiyuan Yang (IME), T.B. Lim (IME), X Dai (HP), Ibrahim Bekar (Intel), and Paul Ho (University of Texas at Austin).

**References**

1. X.J. Fan, "Moisture related reliability in electronic packging", *2005/2006/2007/2008 ECTC Professional Development Course Notes*, 2005/2006/2007/2008
2. G.Q. Zhang, W.D. van Driel, and X.J. Fan, "*Mechanics of Microelectronics*", Springer, 2006
3. X.J. Fan, "Mechanics of moisture for polymers: fundamental concepts and model study", 8th IEEE International Conference on Thermal and Mechanical Simulation and Experiments in Microelectronics and Microsystems, (EuroSimE), April 20-23, 2008
4. A.A.O. Tay, and T.Y. Lin, "Influence of Temperature, Humidity and Defect Location on Delamination in Plastics Packages", *IEEE Transactions on Components, Packaging and Manufacturing Technologies*, Part A, 22, No. 4, pp. 512-518, 1999
5. S. Liu and Y. H. Mei, "Behavior of Delaminated Plastic IC Packages Subjected to Encapsulation Cooling, Moisture Absorption, and Wave Soldering", *IEEE Transactions on Components, Packaging, and Manufacturing Technologies*, Part A, Vol. 18, No. 3, 1995
6. X.J. Fan, G.Q. Zhang, and L.J. Ernst, "Interfacial delamination mechanisms during reflow with moisture preconditioning", *IEEE Transactions of Components and Packaging Technologies*, 2008 (in press)
7. B. Xie, X.Q. Shi, X.J. Fan, and H. Ding, "Direct concentration approach of moisture diffusion and whole field vapor pressure modeling for reflow process", *ASME Journal of Electronic Packaging*, 2008 (submitted)
8. T.Y. Tee, C. Kho, D. Yap, C. Toh, X. Baraton, Z. Zhong, "Reliability assessment and hygroswelling modeling of FCBGA with no-flow underfill" *Microelectronics Reliablity*, 2003, pp. 741-749.
9. H. Ardebili, E.H. Wong, and M. Pecht, "Hygroscopic swelling and sorption characteristics of epoxy molding compounds used in electronic packaging", IEEE Trans. Comp. Packag. Technol., Vol. 26, No. 1 (2003) pp. 206-214.
10. J. Zhou, "Investigation of non-uniform moisture distribution on determination of hygroscopic swelling coefficient and finite element modeling for a flip chip package, *IEEE Transactions of Components and Packaging Technologies*, 2008 (in press)
11. J.W. Osenbach, "Corrosion-induced degradation of microelectronic devices", *Journal of Semicond. Sci. Technol.*, 11, 155-162, 1996
12. Moisture/Reflow Sensitivity Classification for Plastic Integrated Circuit Surface Mount Devices, JEDEC/J-STD-020C, 2004
13. T. Ferguson and J. Qu, "Moisture absorption analysis of interfacial fracture test specimens composed of no-flow underfill materials", *Journal of Electronic Packaging*, Vol. 125, pp 24-30, 2003.
14. S. Luo and C.P. Wong, "Influence of temperature and humidity on adhesion of underfills for flip chip

packaging", *IEEE Transactions of Components and Packaging Technologies* ,Vol. 28, No.1, 88-94, 2005

15. A.G. Evans and J.W. Hutchinson, "The thermomechanical integrity of thin films and multilayers," *Acta. Metall. Mater.*, vol. 43, pp. 2507-2530, 1995
16. J.W. Hutchinson and Z.G. Suo, "Mixed mode cracking in layered materials," *Advances in Applied Mechanics*, 29, pp. 63–191, 1992
17. X.J. Fan, H.B. Wang; & T.B. Lim, "Investigation of the underfill delamination and cracking for flip chip module during thermal cyclic loading", *IEEE Transaction of Component, Manufacturing and Packaging Technology*, 24(1), 84-91, 2001
18. X. Dai, "Materials study for interfacial adhesion and reliability of microelectronics packaging structures", Ph. D. dissertation, University of Texas at Austin, 1998
19. X. Zhang, "Characterization of interfacial adhesion by double cantilever beam metrology", unpublished report, Intel, 2006
20. X.Q. Shi, Y.L. Zhang, W. Zhou, and X.J. Fan, "Effect of hygrothermal aging on interfacial reliability of silicon/underfill/FR-4 assembly", *IEEE Transactions of Components and Packaging Technologies*, 2008 (in press)
21. Eric Stellrecht, Bongtae Han, and Michael G. Pecht, "Characterization of Hygroscopic Swelling Behavior of Mold Compounds and Plastic Packages", IEEE *Transactions on Components and Packaging Technologies*, 27(3), 499-505, 2004
22. Y. He, and X.J. Fan, "In-situ characterization of moisture absorption and desorption in a thin BT core substrate", *Electronic Components and Technology Conference*, pp. 1375-1383, 2007
23. E.H. Wong, K.C. Chan, R. Rajoo, T.B. Lim, "The mechanics and impact of hygroscopic swelling of polymeric materials in electronic packaging," *Proc. 50th Electron. Comp. Technol. Conf.*, Las Vegas, NV, 2000, pp. 576–580.
24. J. Zhou, T.Y. Tee, and J. Luan, "Upper and lower bound theoretical analysis in characterizing hygroscopic swelling of polymeric materials," *38th International Symposium on Microelectronics*, 2005, pp 673-680
25. J. Zhou, T.Y. Tee, and X. Zhang, "Transient analysis on hygroscopic swelling characterization using sequentially coupled moisture diffusion and hygroscopic stress modeling approach," *Proceedings of ASME International Mechanical Engineering Congress and Rd & D Expo*, 2005. IMECE 2005-81847
26. J. Zhou, "Analytical and numerical bound analysis of hygroscopic swelling characterization", *Electronic Components and Technology Conference* , ECTC, 2006
27. X.J. Fan, J. Zhou, G.Q. Zhang and L.J. Ernst, "A micromechanics based vapor pressure model in electronic packages", *ASME Journal of Electronic Packaging*, 127 (3), pp. 262-267, 2005.
28. X.J. Fan, J. Zhou, and G.Q. Zhang, " Multi-physics modeling in virtual prototyping of electronic packages – combined thermal, thermo-mechanical and vapor pressure modeling ", *Journal of Microelectronics Reliability*, 44, 1967-1976, 2004
29. T.Y. Tee and Z.W. Zhong, "Integrated vapor pressure, hygroswelling and thermo-mechanical stress modeling of QFN package during reflow with interfacial fracture mechanics analysis", *Microelectronics Reliability*, Vol. 44(1), pp. 105-114, 2004
30. T.Y. Tee, X.J. Fan and T. B. Lim, "Modeling of whole field vapor pressure during reflow for flip chip and wire-bond PGBA Packages", *1st International Workshop on Electronic Materials & Packaging*, 1999
31. Liu, Y., Irving, S., et al, Simulation and Analysis for Typical Package Assembly Manufacture Process, EuroSimE2006, April, 2006
32. J. Zhou, M. Sitlani, et.al., "Investigation of inner-layer dielectric (ILD) failure by hygroscopic swelling," *IEEE 55th Electronic Components and Technology Conference*, 2005.